Supplementary info – A hybrid integrated dual-microcomb source

Nikita Yu. Dmitriev,[1,2,*] Sergey N. Koptyaev,[3,*] Andrey S. Voloshin,[4,*] Nikita M. Kondratiev,[1,*] Valery E. Lobanov,[1] Kirill N. Min'kov,[1] Maxim V. Ryabko,[3] Stanislav V. Polonsky,[3] and Igor A. Bilenko[1,5]

[1] *Russian Quantum Center, Moscow, 143026, Russia*
[2] *Moscow Institute of Physics and Technology (MIPT), Dolgoprudny, Moscow Region, 141701, Russia*
[3] *Samsung R&D Institute Russia, SAIT-Russia Laboratory, Moscow, 127018, Russia*
[4] *Institute of Physics, Swiss Federal Institute of Technology Lausanne (EPFL), CH-1015 Lausanne, Switzerland*
[5] *Faculty of Physics, M.V. Lomonosov Moscow State University, 119991 Moscow, Russia*

SUPPLEMENTARY NOTE 1: MICROCOMB PARAMETERS REPRODUCIBILITY

In terms of commercially available end-product development for practical applications device characteristics reproducibility and yield ratio are extremely important. Concerning integrated microcomb or dual-comb source considered here least reliable and most unpredictable element, responsible for device performance, is a photonic chip with high-Q SiN microresonator. The process used for photonic chip fabrication has some errors expressed in the deviation of geometric parameters and variation in the material refractive index. Despite such deviations are extremely small in absolute values, it can lead to significant variations in the microresonators' parameters such as coupling rate, microresonator eigenmodes' positions and dispersion characteristics. The microresonators' parameters affect generated microcombs or even significantly complicate its generation. In order to assess the fabrication deviations impact on device performance we examined 7 photonic chips with the same design from different wafer areas. As a result, we successfully generated microcombs using every chip we had and have not even notice significant difference in microcomb generation process from chip to chip. Spectrum of each microcomb was recorded using optical spectrum analyzer (OSA) (Fig.1(a)) and also to distinguish coherent (soliton) state low frequency noise of generated microcombs was observed using electrical spectrum analyzer (ESA) (Fig. 1(b)). Comparison was made for microcombs generated in 1THz microresonators. All generated microcombs feature similar envelope, which indicates to similar dispersion landscape. The maximum observed deviation between microcomb lines position corresponding to same serial number is about 0.9 nm corresponding to ∼112 GHz (Fig. 1(a), inset). Such deviations are usually compensated using powerful micro-heaters or piezo-elements above microresonator, which allows to change its FSR and shift eigenfrequency up to hundreds of GHz [1, 2]. However, micro-heaters used in this experiment enable to shift eigenfrequencies only up to tens of GHz. With regard to this fact, only several photonic chips from the set enable microcombs matching to observe dual-comb signal in RF range.

Thus, we have obtained microcomb generation with photonic chips from different wafer areas and thereby have demonstrated that fabrication process deviations do not lead to inability of microcombs generation in case of using self-injection locked laser diode for pumping. Also, using 1 THz FSR microresonator we have estimated deviations of eigenfrequencies position across the wafer and selected photonic chips which provide microcombs matched to observe RF dual-comb signal.

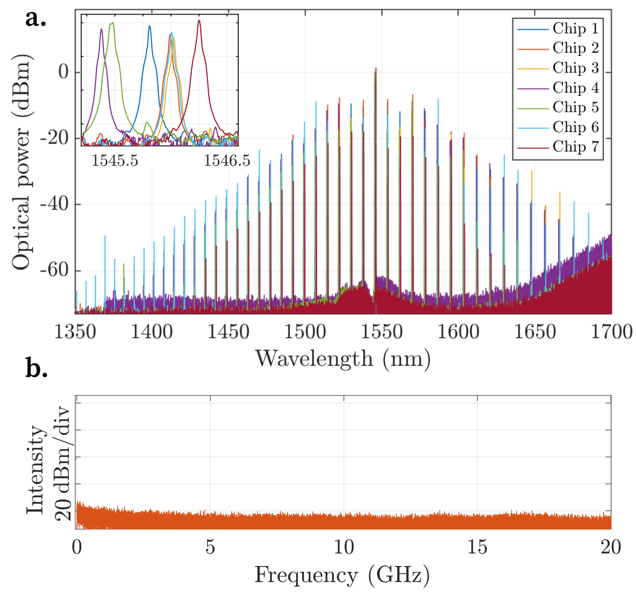

Figure 1. Soliton microcombs generated at different photonic chips **a.** Optical spectra of the generated soliton microcombs at 7 different chips with the same design and pumped with laser diode. Inset: zoom-in of the microcombs central line area. **b.** RF spectrum of the generated microcombs demonstrating the absence of the low frequency noise

SUPPLEMENTARY NOTE 2: LASER DIODES COMPARISON

As a part of conducted experiment, we have compared two different types of laser diodes (LDs), Fabry-Perot (FP) and distributed feedback (DFB), in terms of practical use. Single mode multi-frequency FP diodes manufactured by Seminex Corp., USA, used in the experiment features ∼ 35 GHz longitudinal mode spacing, 1535 nm central wavelength and ∼ 200 mW peak output optical power at 500 mA of the injection current. The single frequency DFB diodes have 1545 nm wavelength, side-mode suppression ratio (SMSR) of $\sim$ -50 dB and peak optical power of $\sim$ 100 mW at 400 mA. Each type of the LDs was used in turn for microcomb generation using the same microresonators. The final results obtained for both types of the LDs looks similar and there was no dramatic differences in generated microcombs' properties. However, during the process of alignment and adjustments of the experimental setup different types of LDs demonstrate extremely different behaviour. Here we describe the features of application for both types of the LDs, as well as present comparative analysis in terms of practical application, describing its advantages and drawbacks.

DFB features single frequency emission, that makes the process of the alignment and microresonator's mode excitation is much more predictable and well managed. Using FP one faces with modes competition and mode-hopping effects, since a number of LD longitudinal mode can be locked to several different microresonator eigenfrequencies. Thus, microcomb generation process with FP LD is much more sensitive to alignment. Any minor translation, which does not affect microcomb generation in case of DFB LD pumping, can cause significant changes due to mode-hopping or even destroy microcomb generation in case of FP LD use.

However, often it is easier to find and excite the mode using exactly FP LD when it comes to microresonator with large FSR, for example 1 THz. Also, as a rule, FP LD in comparison with DFB LD features more output power and higher power efficiency, that sometimes plays a crucial role. Indeed, power is a critical parameter for observing nonlinear effects, such as generation of an optical comb, especially when it comes to complex optical schemes with optical splitters. Moreover, powerful DFB LDs in comparison with FP are much more expensive and less available. In fact, the accessibility, price and interchangeability of elements are very important in the context of the commercial product development.

Thus, it is more expedient to use more affordable and powerful FP diodes for commercial product development and DFB diodes for research purposes on experimental stands in laboratory. Both of these diodes allows "turn-key" comb generation and applicable for packaged device.

SUPPLEMENTARY NOTE 3: SELF-INJECTION LOCKING AND THERMAL EFFECTS

Most of the thermal effects are suppressed as the laser frequency becomes locked to the microresonator and laser-microresonator detuning becomes fixed. If the microresonator frequency is disturbed by the thermal effects, the generation frequency also changes, maintaining the comb generation regime [3]. We repeat this important derivation in more details. The frequency comb generation is described by the nonlinear equation of the form

$$\dot{a}_\mu = -(1 - i\zeta - id_{\Sigma_\mu})a_\mu + iS_\mu + f\delta_\mu, \tag{1}$$

where a is the microresonator mode field, $d_{\Sigma_\mu} = d_2\mu^2 + d_3\mu^3...$ is the integrated dispersion, $\zeta = 2(\omega_{\rm gen} - \omega_0)/\kappa$ is the normalized pump frequency detuning ($\omega_{\rm gen}$ is the generation frequency, ω_0 and κ are the pumped WGM frequency and linewidth), S_μ is the nonlinear sum and f is the normalized pump [4]. If we turn to the thermal-influenced equations they are modified as following [5]:

$$\dot{a}_\mu = -(1 - i\zeta - i\theta - id_{\Sigma_\mu})a_\mu + iS_\mu + f\delta_\mu, \tag{2}$$

$$\dot{\theta} = \tilde{\kappa}_\theta\left(r_\theta P_a - \theta\right), \tag{3}$$

where θ is normalized thermal frequency shift, $\tilde{\kappa}_\theta$ and r_θ are the thermal to optical decay rate and nonlinearity ratios and $P_a = \sum |a_\mu|^2$ is the total intracavity intensity. Comparing equations (1) and (2) we can see that the soliton generation is governed by the effective detuning $\zeta_{\rm eff} = \zeta + \theta$. Note that negative thermorefraction coefficient corresponds to negative r_θ and, consequently negative θ. In stationary regime $\theta = r_\theta P_a$, so we can see that the nonlinear resonance "tilts" to the lower frequencies, while the soliton steps do not shift significantly (the bigger shift, the more the soliton number) and can become inaccessible [5].

In the SIL regime the system should be completed with two more equation systems - for the backward wave amplitudes b_μ (note that the thermal equation should also be modified to have the full microresonator power as a source) and for the laser amplitude a_l. To perform the numerical modeling the laser medium gain model also should be specified (we use the normalized carrier concentration N_g rate equations). The final system can be written as following [3]

$$\frac{dN_g}{d\tau} = \frac{g}{g_0}\frac{f^2}{\tilde{\kappa}^2_{\rm WGR}}(\tilde{\kappa}_l - N_g|a_l|^2) + \tilde{\kappa}_N(\tilde{\kappa}_l - N_g), \tag{4}$$

$$\frac{da_l}{d\tau} = \left(-i\xi_0 - iv_\xi\tau + \alpha_g^c N_g - \tilde{\kappa}_l\right)a_l - \frac{\tilde{K}_0}{f}b_0 e^{-i\psi_s} \tag{5}$$

$$\frac{da_\mu}{d\tau} = -(1 - id_{\Sigma_\mu} - i\theta)a_\mu + i\beta b_\mu + iS^a_\mu + f\delta_{\mu 0}, \tag{6}$$

$$\frac{db_\mu}{d\tau} = -(1 - id_{\Sigma_\mu} - i\theta)b_\mu + i\beta^* a_\mu + iS^b_\mu \tag{7}$$

$$\frac{d\theta}{d\tau} = \frac{\kappa_\theta}{\kappa}\left(r_\theta(P_a + P_b) - \theta\right), \tag{8}$$

where the $\tau = \kappa t/2$ is normalized time, g/g_l is the laser gain to Kerr nonlinearity rate ratio, $\tilde{\kappa}_{\rm WGR}$ is the coupling of the microresonator normalized to the microresonator mode linewidth, $\tilde{\kappa}_l$ and $\tilde{\kappa}_N$ are the laser field and carrier relaxation rates normalized to the microresonator mode linewidth, $\alpha_g^c = (1 + i\alpha_g)$ and α_g is the Henry factor, ψ_s is the locking phase, ξ_0 is the initial laser detuning and $v_\xi = v_f[\text{Hz/s}]\frac{8\pi}{\kappa^2}$ is the scan speed in half-linewidth per reversed half-linewidth, $\tilde{K}_0 = \frac{K_0}{2\beta\sqrt{1+\alpha_g^2}}$ is the resonator to laser coupling coefficient, defined by the stabilization coefficient, $K_0 = 8\eta\beta\tilde{\kappa}_{do}$ is the zero-detuning stabilization coefficient, $\tilde{\kappa}_{do}$ is the ratio of the laser output mirror coupling rate to the WGM linewidth, β is the normalized scattering rate in microresonator. It can be noted that K_0 also approximately equal to triple locking width in units of WGM linewidth in linear regime. Solving these equations numerically one may see that the generated comb regime does not depend on the value of the thermal nonlinearity up to significant values.

Some more insight can be obtained using the tuning curve approach [6]. We can see [3] that the resulting tuning curve for $\zeta_{\rm eff}$ coincides with the solution without thermal influence. Using nonlinear shifts $\bar\zeta = \zeta_{\rm eff} + \delta\zeta_{\rm nl}$, $\bar\beta^2 = \delta\beta^2_{\rm nl} + \beta^2$ and $\bar\xi = \xi + \delta\zeta_{\rm nl}$ for the tuning curve over the laser cavity detuning ξ we can obtain an implicit expression[7]:

$$\delta\beta_{\rm nl} = \frac{2\alpha_x - 1}{2}|f|^2 \frac{1 + (\bar\zeta + \delta\beta_{\rm nl})^2 - \beta^2}{(1 + \bar\beta^2 - \bar\zeta^2)^2 + 4\bar\zeta^2}, \quad (9)$$

$$\xi = \zeta_{\rm eff} + \frac{K_0}{2}\frac{2\bar\zeta\cos\bar\psi + (1 + \bar\beta^2 - \bar\zeta^2)\sin\bar\psi}{(1 + \bar\beta^2 - \bar\zeta^2)^2 + 4\bar\zeta^2}, \quad (10)$$

$$\zeta_{\rm eff} = \bar\zeta - \frac{2\alpha_x + 1}{2}|f|^2 \frac{1 + (\bar\zeta + \delta\beta_{\rm nl})^2 + \beta^2}{(1 + \bar\beta^2 - \bar\zeta^2)^2 + 4\bar\zeta^2}, \quad (11)$$

where $\bar\psi = \psi_0(\omega_m\tau_s) + \frac{\kappa\tau_s}{2}\zeta$ is the locking phase (τ_s is the roundtrip time from the laser to the microresonator). From the equations (10)-(11) we can see that exactly the $\zeta_{\rm eff}$ is the detuning that is stabilized, while the generation detuning ζ will follow the temperature change. Furthermore, in the locked state this detuning becomes fixed to the detuning near

$$\zeta^0_{\rm eff} = \begin{cases} -\frac{3}{2}f^2, & f \ll 1 \\ -3\left(\frac{f^2}{2}\right)^{1/3} + \left(\frac{f^2}{2}\right)^{-1/3}, & f > 1 \end{cases} \quad (12)$$

This expression is obtained for $\alpha_x = 1$, low $\beta \ll 1$ and $\bar\psi = 0$. We choose $\bar\zeta = 0$, which guarantees it being in the locked state. This is a good estimation if the pump is not very high ($f < 2$), where the tuning and resonance curves are more-or-less symmetric, without self-intersections and good stabilization can be achieved. The sample solutions of (10)-(11) for different f are shown in Supplementary Fig. 2. It can be shown that $\zeta^0_{\rm eff}$ always lies inside the soliton generation region $\zeta_{\rm eff} \in [-3(f/2)^{2/3} + (f/2)^{-2/3}/4; -\pi^2 f^2/8]$ [8, 9]. Unfortunately, the lower boundary of the soliton existence region approximation is not very good near $f = 1$ as they are based on the resonance curve bistability, which appears only after $f = 1.24$.

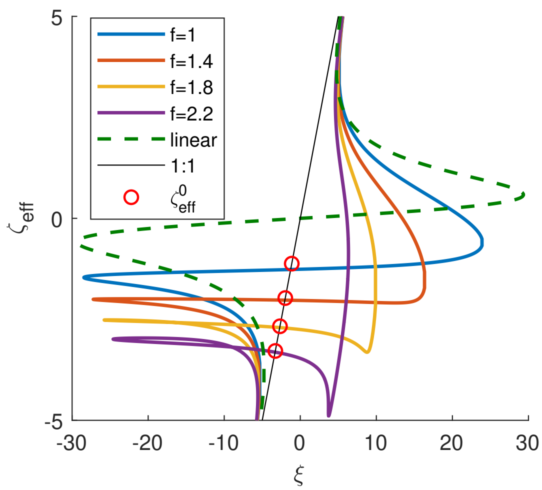

Figure 2. Sample solutions of (10)-(11) for different pump amplitude f for parameters $\alpha_x = 1$, $\bar\psi = 0$, $\beta = 0.11$, $K_0 = 88$ together with locked effective detunings (12) (red circles).

SUPPLEMENTARY NOTE 4: COMB ENVELOPE APPROXIMATION AND POWER EFFICIENCY

The generated comb for single soliton can be calculated as following [10]:

$$a_\mu = \sqrt{\frac{d_2}{2}}\,\mathrm{sech}\left(\frac{\pi\mu}{2}\sqrt{\frac{d_2}{-\zeta_{\rm eff}}}\right)e^{i\psi^{\rm sol}} \quad (13)$$

$$\psi^{\rm sol} = \arctan\frac{\sqrt{-2\pi^2 f^2\zeta_{\rm eff} - 16\zeta^2_{\rm eff}}}{-4\zeta_{\rm eff}}. \quad (14)$$

Note that the total comb (or soliton) power $P_{\rm soliton} = 2\sqrt{-\zeta_{\rm eff}d_2}/\pi$ does not depend on the pump amplitude

$$f = \sqrt{\frac{8g}{\kappa^3}}\sqrt{\frac{\eta\kappa}{\tau_{\rm WGM}}}A_l|_{\rm coupler} = \sqrt{\frac{8cn_2Q^2\eta P_{\rm coupler}}{\omega n_g^2 V_{\rm eff}}}, \quad (15)$$

meaning that the higher the pump, the lower the comb generation efficiency. In the formula g is nonlinearity rate, κ is the WGM linewidth, $\eta = \kappa_c/\kappa$ is the normalized coupling rate, $\tau_{\rm WGM}$ is the WGM round-trip time, $A_l|_{\rm coupler}$ and $P_{\rm coupler}$ are the pump field amplitude and power inside the coupler, n_2 is the nonlinear index, Q is the loaded quality factor, n_g is the WGM group index, $V_{\rm eff}$ is the WGM mode volume. It is convenient to introduce the parametric instability threshold power $P_{\rm th}$, so that $f = \sqrt{P_{\rm coupler}/P_{\rm th}}$. Upon reaching this power the nonlinear generation process starts. To turn to the output comb amplitude we have to recall the nonlinearity normalization

$$A^{\rm out}_\mu = -\sqrt{\eta\kappa\tau_{\rm WGM}}a_\mu\sqrt{\frac{\kappa}{2g}} = \frac{2\eta}{f}a_\mu A_l|_{\rm coupler}. \quad (16)$$

Using the threshold power we can write out a simple expression for the output comb line power in the form

$P_\mu^{\rm out} = 4\eta^2|a_\mu|^2 P_{\rm th}$ and the total power

$$P_{\rm soliton}^{\rm out} = \frac{8\eta^2}{\pi}\sqrt{-d_2\zeta_{\rm eff}}P_{\rm th}. \quad (17)$$

This brings out an nontrivial fact that lowering the threshold power also reduces the output comb power.

The central line in the output light also interferes with the background of nonlinear resonance curve

$$A_{\rm CW}^{\rm out} = \left(1 - \frac{2\eta}{1 - i\zeta_{\rm eff} - ia_{\rm CW}^2}\right) A_l|_{\rm coupler}, \quad (18)$$

and $A_{\rm CW}^2$ is the squared absolute value of the stationary nonlinear resonance. In our case we take the lower branch of bistability region

$$a_{\rm CW}^2 = -\frac{2}{3}\zeta_{\rm eff} - \frac{2}{3}\sqrt{\zeta_{\rm eff}^2 - 3}\times \cosh\frac{1}{3}\operatorname{arccosh}\frac{-2\zeta_{\rm eff}^3 - 18\zeta_{\rm eff} - 27f^2}{2(\zeta_{\rm eff}^2-3)^{3/2}} \quad (19)$$

The power efficiency can be calculated in two ways. First is the "pump to total comb" or "pump to solitons" ($\eta_{\rm p2s}$) efficiency [11, 12], where the total comb power (17) is divided by the pump power in the coupler $P_{\rm coupler}$. It is usually used in theoretical calculations giving out more tidy formulas. The second way can be referred to as "pump to comb sidebands" or "pump to comb" ($\eta_{\rm p2c}$), when the central (pumped) line is excluded [13]:

$$\eta_{\rm p2c} = \frac{4\eta^2}{f^2}\left(\sum|a_\mu|^2 - |a_0|^2\right) = \frac{4\eta^2}{f^2}\left(\frac{2}{\pi}\sqrt{-d_2\zeta_{\rm eff}} - \frac{d_2}{2}\right), \quad (20)$$

where the first summand is effectively "pump to solitons" $\eta_{\rm p2s}$ efficiency and the subtracted term is the central line power. This is convenient in experiment not to bother with the interference with the pump. It can also be more informative for those more interested in sideband power than in the total comb power. In the main article we use this variant. At maximum detuning $\zeta_{\max} = -\pi^2 f^2/8$ the first summand of (20) is

$$\eta_{\rm p2s}^{\max} \approx \frac{4\eta^2}{f}\sqrt{\frac{d_2}{2}} = \eta^{3/2}\sqrt{\frac{d_2\kappa n_g^2 V_{\rm eff}}{cn_2 Q P_{\rm coupler}}}, \quad (21)$$

which coincides with expression for pump-to-soliton efficiency in [11, 12]. We can see that even at maximum detuning, that grows with the pump amplitude, the power efficiency scales down. In the SIL regime the efficiency is lower as the detuning is locked to lower value (12). Nevertheless the high efficiency can be maintained due to the possibility of lower pump power usage.

The self-injection locking usually leads to the multi-soliton state, which also increases the pump-to-comb efficiency. To model the N-soliton comb we multiply the (13) with

$$\Phi_\mu = \sum_{k=1}^{N}\exp i\mu\phi_k, \quad (22)$$

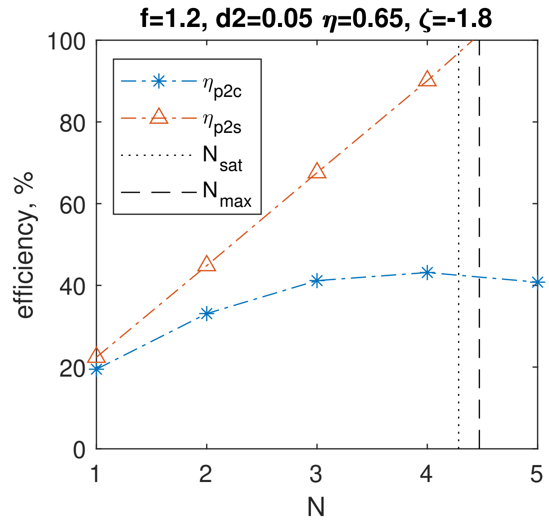

Figure 3. Pump to soliton (21) and pump to comb sidebands (20) efficiency dependence on the soliton number for parameters, close to 1 THz chip. The former is shown with red triangles, the latter – with blue asterisk. Vertical dashed and dotted lines show the 5-width and maximum soliton number respectively.

where ϕ_k is the k-soliton angle position on the circumference. If the solitons are equidistant (so-called perfect solitonic crystal [14]) the comb will have N-FSR spacing. However, if the solitons have random angle distribution we get 1-FSR spaced comb and its sech^2 envelope experience non-smooth modulation. The total comb power (and the pump-to-comb efficiency) grows linearly with the number of solitons until the mutual distance between them is less than 5 soliton widths ($N_{\rm sat} \approx 2\pi/(10\sqrt{-d_2/\zeta_{\rm eff}}\operatorname{arccosh}\sqrt{2})$) [10]. Up to this moment the pump-to-sidebands efficiency saturates (see Supplementary Fig. 3). We should also note that this number is usually inaccessible as the detuning is usually scanned from red to blue side and the soliton formation occurs at low ζ and their number does not grow. So the practical estimation for maximum soliton number would be $N_{\max} \approx \sqrt{1/d_2}$ [14].

To sum up this section, the comb power does not depend on the pump power directly. Though both the maximal and the locked detunings do depend on the pump power, these dependencies are weaker than the linear one and the pump-to-comb efficiency decreases with it. This creates the illusion that using the low power laser and reducing the threshold we can make a very energy-efficient device. However, the second point is that the comb power does depend on the nonlinearity threshold power. So, using the above strategy we end up with negligible output signal. This brings us to rather counter-intuitive conclusion, that for best performance the threshold power should be increased (meaning lower Q-factors or less nonlinearity, for example) and matched with the used laser pump power. This immediately brings out a trade-off problem as the lower Q-factor means less stabilization and wider beatnote. Another way to increase the pump-to-comb efficiency is the second order dispersion coefficient increase. Unfortunately, this brings us to a trade-off problem for the comb width.

---

* These authors contributed equally to this work.

[1] X. Xue, Y. Xuan, C. Wang, P.-H. Wang, Y. Liu, B. Niu, D. E. Leaird, M. Qi, and A. M. Weiner, Opt. Express **24**, 687 (2016).

[2] J. Liu, H. Tian, E. Lucas, A. S. Raja, G. Lihachev, R. N. Wang, J. He, T. Liu, M. H. Anderson, W. Weng, S. A. Bhave, and T. J. Kippenberg, Nature **583**, 385 (2020).

[3] N. M. Kondratiev, R. R. Galiev, and V. E. Lobanov, in *Nonlinear Optics and Applications XII*, Vol. 11770, edited by M. Bertolotti, A. V. Zayats, and A. M. Zheltikov, International Society for Optics and Photonics (SPIE, 2021) pp. 53 – 58.

[4] N. M. Kondratiev, V. E. Lobanov, E. A. Lonshakov, N. Y. Dmitriev, A. S. Voloshin, and I. A. Bilenko, Opt. Express **28**, 38892 (2020).

[5] H. Guo, M. Karpov, E. Lucas, A. Kordts, M. H. P. Pfeiffer, V. Brasch, G. Lihachev, V. E. Lobanov, M. L. Gorodetsky, and T. J. Kippenberg, Nature Physics **13**, 94 (2016).

[6] N. M. Kondratiev, V. E. Lobanov, A. V. Cherenkov, A. S. Voloshin, N. G. Pavlov, S. Koptyaev, and M. L. Gorodetsky, Opt. Express **25**, 28167 (2017).

[7] A. S. Voloshin, N. M. Kondratiev, G. V. Lihachev, J. Liu, V. E. Lobanov, N. Y. Dmitriev, W. Weng, T. J. Kippenberg, and I. A. Bilenko, Nature Communications **12**, 235 (2021).

[8] N. M. Kondratiev and V. E. Lobanov, Phys. Rev. A **101**, 013816 (2020).

[9] C. Godey, I. V. Balakireva, A. Coillet, and Y. K. Chembo, Phys. Rev. A **89**, 063814 (2014).

[10] T. Herr, V. Brasch, J. D. Jost, C. Y. Wang, N. M. Kondratiev, M. L. Gorodetsky, and T. J. Kippenberg, Nat. Photon. **8**, 145 (2014).

[11] C. Bao, L. Zhang, A. Matsko, Y. Yan, Z. Zhao, G. Xie, A. M. Agarwal, L. C. Kimerling, J. Michel, L. Maleki, and A. E. Willner, Opt. Lett. **39**, 6126 (2014).

[12] J. K. Jang, Y. Okawachi, Y. Zhao, X. Ji, C. Joshi, M. Lipson, and A. L. Gaeta, Opt. Lett. **46**, 3657 (2021).

[13] X. Xue, P.-H. Wang, Y. Xuan, M. Qi, and A. M. Weiner, Laser & Photonics Reviews **11**, 1600276 (2017).

[14] M. Karpov, M. H. P. Pfeiffer, H. Guo, W. Weng, J. Liu, and T. J. Kippenberg, Nature Physics **15**, 1071 (2019).